

LIFTING THE VEIL OF DUST FROM NGC 0959: THE IMPORTANCE OF A PIXEL-BASED 2D EXTINCTION CORRECTION

K. TAMURA¹, R. A. JANSEN^{2,1}, P. B. ESKRIDGE^{2,3}, S. H. COHEN², AND R. A. WINDHORST^{2,1}
(Accepted for publication in *Astronomical Journal*, April 14, 2010)

ABSTRACT

We present the results of a study of the late-type spiral galaxy NGC 0959, *before* and *after* application of the pixel-based dust extinction correction described in Tamura et al. 2009 (Paper I). *Galaxy Evolution Explorer* (GALEX) far-UV (FUV) and near-UV (NUV), ground-based Vatican Advanced Technology Telescope (VATT) *UBVR*, and *Spitzer*/Infrared Array Camera (IRAC) 3.6, 4.5, 5.8, and 8.0 μm images are studied through pixel Color-Magnitude Diagrams (pCMDs) and pixel Color-Color Diagrams (pCCDs). We define groups of pixels based on their distribution in a pCCD of $(B - 3.6 \mu\text{m})$ versus $(\text{FUV} - U)$ colors *after* extinction correction. In the same pCCD, we trace their locations *before* the extinction correction was applied. This shows that selecting pixel groups is not meaningful when using colors uncorrected for dust. We also trace the distribution of the pixel groups on a pixel coordinate map of the galaxy. We find that the pixel-based (two-dimensional) extinction correction is crucial to reveal the spatial variations in the dominant stellar population, averaged over each resolution element. Different types and mixtures of stellar populations, and galaxy structures such as a *previously unrecognized* bar, become readily discernible in the extinction-corrected pCCD and as coherent spatial structures in the pixel coordinate map.

Subject headings: dust, extinction — galaxies: individual (NGC 0959) — galaxies: spiral — galaxies: stellar content — galaxies: structure

1. INTRODUCTION

Studying the distribution of different stellar populations within galaxies is crucial to understand the formation and evolutionary history of galaxies. One of the obstacles that prevents us from directly observing these stellar populations is the attenuation and reddening by dust that is randomly distributed among, or projected along the line-of-sight toward, these stellar populations. This has remained a major problem for nearly a century (e.g., Trumpler 1930; Mathis et al. 1977; Viallefond et al. 1982; Caplan & Deharveng 1985; Witt et al. 1992; Roussel et al. 2005; Driver et al. 2008). While the main effect of dust is to attenuate the light emitted by stars, dust also scatters light out of the line-of-sight, and may re-direct light from nearby regions into our line-of-sight (e.g., Witt et al. 1992; Witt & Gordon 1996, 2000). The impact of extinction—the wavelength-dependent net effect of absorption and scattering—correlates with the spatial distribution of star-forming regions (e.g., Waller et al. 1992; Deo et al. 2006), as it depends on both the geometry of the dust distribution (e.g., Elmegreen 1980; Walterbos & Kennicutt 1988; Calzetti et al. 1994; Witt & Gordon 1996, 2000) and on the physical and chemical properties of the dust (e.g., van Houten 1961; Witt et al. 1992; Whittet et al. 2001, 2004). On typical observational scales, the dust will be intermixed with the stellar populations as thin layers, filaments, and dense clumps. Even though some light may be scattered into the line-of-sight from the rear and from regions near the

line-of-sight, most of the extinction by far will be due to dust that is distributed *in front* of the stellar populations of interest (Byun 1992).

Popular methods to measure dust extinction, such as the use of Hydrogen recombination line ratios (e.g., Rudy 1984; Scoville et al. 2001; Calzetti et al. 2005, 2007; Kennicutt et al. 2009), the ultraviolet (UV) spectral slope (e.g., Calzetti et al. 1994; Kong et al. 2004), or ratios of the UV and total infrared fluxes (e.g., Buat & Xu 1996; Calzetti et al. 2000; Boissier et al. 2004, 2005), have various constraints and limitations (e.g., Xu & Helou 1996; Petersen & Gammelgaard 1997; Regan 2000; Price et al. 2002; Boissier et al. 2004; Rieke et al. 2004). In Tamura et al. (2009, hereafter Paper I), we introduced a new method to measure the dust extinction in galaxies, and demonstrated that the spatial distribution of dust extinction in a late-type spiral galaxy, NGC 0959, can be mapped using only the *flux ratio of optical V-band and mid-infrared (mid-IR) 3.6 μm images*. In the present paper, we present the results of a multi-wavelength (UV–optical–mid-IR) study of the effect of the pixel-based two-dimensional extinction correction of Paper I on color composite images, a pixel Color–Color Diagram (pCCD), and a pixel coordinate map of NGC 0959. These results show that a detailed pixel-based extinction correction is essential to reveal the nature and distribution of stellar populations in galaxies.

2. ASSUMPTIONS ABOUT DUST EXTINCTION

Even though the effects of dust attenuation dominate over those by scattering, scattering cannot be ignored completely. Witt & Gordon (1996, 2000) show that, depending on dust geometry, the effect of scattering can be significant. Among the modeled dust geometries, their CLOUDY model corresponds closest to the dust geometry we assumed in Paper I: a geometry where thin layers,

Electronic address: ktamura@asu.edu

¹ Department of Physics, Arizona State University, Tempe, AZ 85287-1504, USA² School of Earth and Space Exploration, Arizona State University, Tempe, AZ 85287-1404, USA³ Department of Physics and Astronomy, Minnesota State University, Mankato, MN 56001, USA

filaments, and dense clumps of dust are intermixed with the stars. Witt & Gordon (2000, their Figure 8) find that this model shows the smallest effect from scattering, with $F_{\text{scat}}/F_* \lesssim 0.1$ (or $\Delta\mu \lesssim 0.1 \text{ mag arcsec}^{-2}$, in agreement with Byun 1992) for all modeled wavelengths ($\lambda > 0.1 \mu\text{m}$) and metallicities, even for very clumpy dust distributions.

While Witt & Gordon (1996, 2000) model the effect of dust attenuation and scattering, Gordon et al. (2003)—and references therein—measured the UV–near-IR extinction toward different regions within the Milky Way (MW), the Large Magellanic Cloud (LMC), and the Small Magellanic Cloud (SMC). Since the effects of attenuation and scattering cannot be separated, the observed extinction curves in Gordon et al. (2003) are the total effect of dust. Similarly, the extinction measured in Paper I represents the total, or net, effect of both attenuation and scattering.

One needs to adopt an extinction curve to scale the measured visual extinction, A_V , to the extinction A_λ in other bandpasses. There appears to be a systematic change from an SMC (Gordon & Clayton 1998) via an LMC (Misselt et al. 1999) to a MW type (Clayton et al. 2000; Valencic et al. 2003) extinction curve, which—while controversial and unproven—is often taken to reflect the difference in average metallicity and/or morphology of these galaxies. Even within a single galaxy, however, there is significant variation between extinction curves derived for different sightlines toward individual stars or regions (e.g., Gordon & Clayton 1998; Misselt et al. 1999; Clayton et al. 2000; Valencic et al. 2003; Gordon et al. 2003). The rapid decrease in attainable spatial resolution with increasing distance renders similar measurements impossible for galaxies beyond the Local Group. Based on its overall morphology and luminosity, we assumed in Paper I that an LMC-like extinction curve—actually the “LMC2 supershell” extinction curve of Gordon et al. (2003)—would be more appropriate for NGC 0959 than either an SMC or MW-type extinction curve. At the $\simeq 10$ Mpc distance of NGC 0959, we expect that the mixing of light from neighboring stellar populations on ~ 250 pc scales will tend toward a mean similar to that for the LMC2 supershell, even when the extinction toward individual stellar populations might be better characterized by an SMC or MW-type extinction curve. Adopting the SMC bar (Gordon et al. 2003) or an average MW-extinction curve, would over- or under-estimate the extinction at shorter wavelengths, respectively.

3. DATA-SET AND PREPARATION

The galaxy selected for this pilot study, NGC 0959, is a late-type spiral galaxy (Sdm; de Vaucouleurs et al. 1991) at a distance of $D = 9.9 \pm 0.7$ Mpc (Mould et al. 2000) with an inclination of $\sim 50^\circ$ (Esipov et al. 1991). This galaxy has been observed with *GALEX* (Martin et al. 2005; Morrissey et al. 2007) in the FUV and near-UV (NUV), with the Vatican Advanced Technology Telescope (VATT) in *UBVR* from the ground (Taylor et al. 2005), and with *Spitzer*/IRAC in the 3.6, 4.5, 5.8, and 8.0 μm filters (Fazio et al. 2004). Near-IR *JHK_s* images are also available from the Two Micron All Sky Survey (2MASS; Skrutskie et al. 2006), but these near-IR images are too shallow for our purpose, and therefore excluded from the analysis. All displayed images and pixel-maps

are rotated such that North is up and East is to the left. The surface brightness and colors are in units of mag arcsec^{-2} and mag , respectively, and are on the AB magnitude system (Oke 1974; Oke & Gunn 1983).

To perform the pixel-based analysis, all images are convolved and re-sampled to a matching point spread function (PSF) and pixel scale. Among all images from the different telescopes and instruments of interest, the coarsest pixel scale and PSF are $1''.5 \text{ pixel}^{-1}$ and $\sim 5''.3$ FWHM, respectively, for the *GALEX* NUV image. IDL⁴ function “*frebin*” (with its flux conserving option switched on) and IRAF⁵ routine “*gauss*” (with a round two-dimensional Gaussian convolution kernel) are used to match the pixel scale and PSF at all wavelengths, while conserving the total amount of surface flux. We then select only those pixels that have a signal-to-noise (S/N) ≥ 3.0 in all filters for further analysis, ensuring reliable pixel surface brightness measurements and colors. Below, we briefly describe the data used in this analysis. For the details of the data preparation and the method of extinction correction we refer the reader to Paper I.

3.1. *GALEX* Images

The *GALEX* FUV and NUV images are obtained from the Multi-Mission Archive at the Space Telescope Science Institute⁶ (MAST). NGC 0959 was observed in the *GALEX* All-sky Imaging Survey (AIS; Martin et al. 2005) and the *GALEX* Nearby Galaxy Survey (NGS; Gil de Paz et al. 2007). Since the galaxy is barely visible in the AIS images, we will use only the deeper (~ 1695 sec) NGS data for our analysis, focusing only on a $7''.5 \times 7''.5$ image section centered on NGC 0959. Since the average FWHM of stars near NGC 0959 is larger in the NUV image (e.g., Martin et al. 2005), we convolve the FUV image to match the PSF in the NUV.

3.2. Ground-based Images

Ground-based *UBVR* images were obtained by Taylor et al. (2005) with the direct CCD imager at the VATT at Mt. Graham International Observatory (MGIO) in Arizona. These flux calibrated images are available through the NASA/IPAC Extragalactic Database⁷ (NED). For a detailed description of this data-set, we refer the reader to Taylor et al. (2005), and references therein. The effective exposure times in *U*, *B*, *V*, and *R* are 1200, 600, 480, and 360 sec, respectively. The native resolution and pixel scale are $\sim 1''.3$ (FWHM) and $0''.37 \text{ pixel}^{-1}$. These images are registered, convolved and resampled to match the orientation, PSF, and pixel scale of the *GALEX* NUV image.

⁴ IDL is distributed by ITT Visual Information Solutions (Research System Inc.), Boulder, Colorado: <http://rsinc.com/idl/>

⁵ IRAF is distributed by National Optical Astronomy Observatory (NOAO), which is operated by the Association of Universities for Research in Astronomy (AURA), Inc., under cooperative agreement with National Science Foundation (NSF): <http://iraf.net/>

⁶ Galaxy Evolution Explorer, GR4 Data Release (May 1, 2009): <http://galex.stsci.edu/GR4/>

⁷ NASA/IPAC Extragalactic Database: <http://nedwww.ipac.caltech.edu/>

3.3. Spitzer/IRAC Images

The *Spitzer*/IRAC 3.6–8.0 μm pipeline-product images were obtained from the *Spitzer* Archive⁸ via *Leopard*. For each filter, the mosaiced image was created with an effective exposure time of 26.8 sec. The native pixel scale is $1''.2 \text{ pixel}^{-1}$, and the effective resolution (FWHM) ranges from $\sim 2''.2$ at 3.6 μm to $\sim 2''.3$ at 8.0 μm . Like for the VATT images, we match the orientations, PSF, and pixel scale of the IRAC images to those of the *GALEX* NUV image.

4. CONSTRUCTING AN EXTINCTION MAP OF NGC 0959

In Paper I, we estimated the visual dust extinction (A_V in mag arcsec^{-2}) measured over each $1''.5 \times 1''.5 \simeq 72 \times 72 \text{ pc}^2$ pixel in NGC 0959 as follows. From histograms of the observed visual to 3.6 μm flux ratio ($f_V/f_{3.6\mu\text{m}}$) in each pixel, we estimate the intrinsic extinction-free flux ratios ($\beta_{V,0}$) for two groups of pixels: pixels apparently dominated by the light from younger and pixels apparently dominated by the light from older stellar populations. These are separable based on their distribution pattern in a pCMD of the observed μ_V versus ($U - 3.6 \mu\text{m}$) color. Since the mid-IR 3.6 μm flux is assumed to be minimally affected by the dust, and hence usually treated as extinction-free (e.g., Fazio et al. 2004; Willner et al. 2004), A_V in each pixel can be inferred from the difference between the *observed* ($f_{V,\text{obs}}$) and *estimated* extinction-free (i.e., $f_{V,0} = \beta_{V,0} \times f_{3.6\mu\text{m,obs}}$) V -band fluxes. For further details of the method, we refer the reader to Paper I. The extinctions in other bandpasses (*GALEX* NUV and FUV, and optical U , B , and R bands) are then scaled from A_V using the adopted LMC2 supershell extinction curve of Gordon et al. (2003).

In Figure 1, the extinction map of NGC 0959 thus produced, darker grayscales correspond to higher values of A_V . The grayscales saturate for $A_V \geq 0.4 \text{ mag arcsec}^{-2}$ (indicated by the white vertical line in the color bar) to enhance the visibility of the lower A_V values in the galaxy, and so differ from that of Figure 10(a) in Paper I. The maximum extinction measured in this galaxy, averaged over a pixel, is $A_{V,\text{max}} \simeq 0.8 \text{ mag arcsec}^{-2}$.

5. LIFTING THE VEIL OF DUST FROM NGC 0959

5.1. Color Composite Images

To visually (qualitatively) investigate the effect of our pixel-based extinction correction on an image of NGC 0959, we first construct two color composites of the galaxy, composed of the *Spitzer*/IRAC 3.6 μm (red channel), the ground-based V (green channel), and the *GALEX* FUV (blue channel) images. Figures 2(a) and 2(b) show the color composites *before* and *after* extinction correction. The image resolutions are matched to that of the *GALEX* NUV image. For easy comparison, both images were created using the *same* color stretch, and with the IRAC 8.0 μm contours over-plotted.

In Figure 2(a), there are several regions in the galaxy that appear much redder than other parts of the galaxy. These regions include: (a) the southern half of the galaxy, especially along the southern “edge” of the galaxy disk (as defined by our $S/N_{\text{min}} = 3.0$ requirement in each of

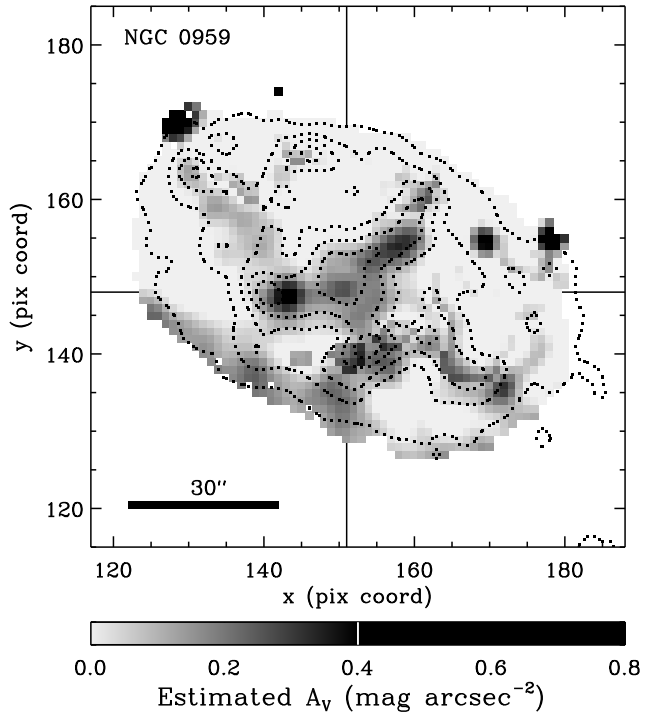


FIG. 1.— Spatial distribution of the pixel-averaged visual dust extinction, A_V . Extinction values map onto grayscales from light-gray ($A_V = 0$) to black ($A_V = 0.4 \text{ mag arcsec}^{-2}$; indicated by a white vertical line in the color bar). The few pixels with $0.4 \leq A_V \leq 0.8 \text{ mag arcsec}^{-2}$ are also rendered as black. Dotted contours trace the *Spitzer*/IRAC 8.0 μm PAH emission and show good agreement with the visual extinction estimates, which were inferred from the observed V -band and 3.6 μm fluxes only. The map measures $\sim 135'' \times 120''$, has a plate scale of $1''.5 \text{ pixel}^{-1}$, and has North up and East to the left.

the filters); (b) the strong 8.0 μm emission region that is running from NW to SE of the galaxy through its center, appearing especially redder at its northern end point; and (c) some localized regions at the north-western and eastern edge of the galaxy disk. Since dust features are not resolved at *GALEX* resolution, we cannot tell whether these pixels in Figure 2(a) are red due to extinction, or are dominated by intrinsically red stellar populations. From the distribution of the estimated visual dust extinction A_V (Figure 1), however, we infer that these red pixels are indeed red due to intervening dust at these locations.

After applying our extinction correction, Figure 2(b) shows that many of the strikingly red pixels in Figure 2(a) indeed have become bluer. Especially regions (b) and (c) have become much bluer than before, while some of the regions (a) still seem to have relatively red colors compared to other parts of NGC 0959’s disk. There are some other regions which have become much bluer as well—mostly located in the SW region and northern regions of the galaxy. These regions already had a relatively blue hue in Figure 2(a), but became much bluer and brighter after extinction correction. They likely are actively star-forming regions.

To see whether these red and blue regions in Figure 2 actually correspond to dust features and SF-regions, we created a third color composite image with a higher spatial resolution from the ground-based *UVR* images at

⁸ *Spitzer* Science Center (SCC) Data Archives/Analysis: <http://ssc.spitzer.caltech.edu/archanaly>

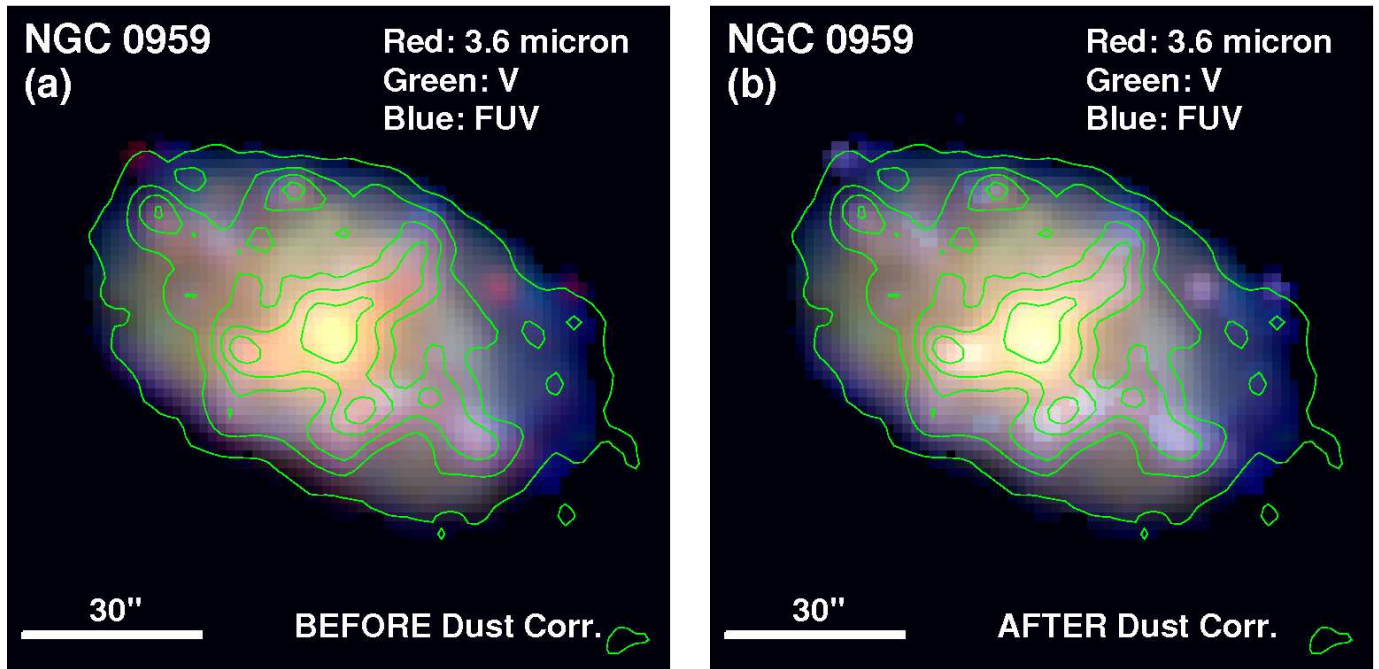


FIG. 2.— Color composite images of NGC 0959 using images from *Spitzer*/IRAC $3.6\ \mu\text{m}$ (red), VATT V (green), and *GALEX* FUV (blue) at *GALEX* resolution (a) before and (b) after application of our pixel-based dust-extinction correction (Paper I). The *Spitzer*/IRAC $8.0\ \mu\text{m}$ emission is over-plotted as green contours. Both color composites are created using the same color stretch. Regions corresponding to high A_V values in Figure 1 clearly become much bluer after extinction correction (panel b). This is especially clear in the blue star-forming knots which generally coincide with peaks in the *Spitzer* $8.0\ \mu\text{m}$ emission.

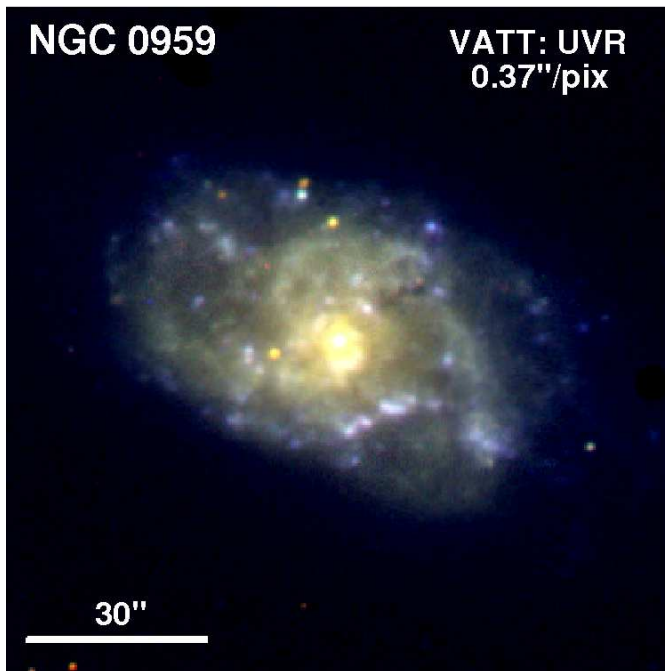


FIG. 3.— Color composite image of NGC 0959 using VATT U , V , and R images at their native ground-based resolution ($\text{FWHM} \approx 1''.3$) and pixel scale ($0''.37\ \text{pixel}^{-1}$) and without any extinction correction. Some dust features and blue star forming regions are readily discernible.

their native resolution and pixel scale of $\text{FWHM} \approx 1''.3$ (matched across UVR) and $0''.37\ \text{pixel}^{-1}$. Figure 3 shows that the blue regions that become bluer and brighter are indeed likely SF-regions. It also shows that the redder pixels in region (b) described above seem to be caused by thick dust lanes running from the NW to SE

in the galaxy. It is hard to see whether regions (a) and (c) are caused by a dust lane or not, but regions (a) seems to be distributed around bluer clumps in Figure 3. The localized regions (c) do not appear to be unrelated background or foreground objects. Such objects usually have colors sufficiently different from those of the genuine galaxy pixels, that they would appear as a distinct and separate branch or grouping of pixels in pCMDs and pCCDs. Since we found no such feature in the examined pCMDs and pCCDs for NGC 0959 (e.g., Figure 4), we treat these regions as parts of the galaxy.

5.2. A ($B - 3.6\ \mu\text{m}$) versus ($FUV - U$) pCCD

To study the effect of our pixel-based extinction correction in a more quantitative way, we examined pCMDs and pCCDs using various combinations of images from FUV through $8.0\ \mu\text{m}$ for significant features or groupings in the pixel-distribution. A distinct grouping of pixels in these diagrams should indicate that those pixels are dominated by the same or a similar mix of stellar populations. Among different diagrams examined (not shown here), a pCCD of ($B - 3.6\ \mu\text{m}$) versus ($FUV - U$) color after extinction correction (Figure 4(a)) was selected, because it clearly shows distinct tracks and groupings of pixels. In particular, distinct red and blue sequences can be identified.

The uncertainties in the colors at the 25th and 75th percentiles are ~ 0.01 and ~ 0.02 mag in ($FUV - U$), and ~ 0.05 and ~ 0.08 mag in ($B - 3.6\ \mu\text{m}$), respectively. Since the gap of ~ 0.2 mag at the bluer end of ($FUV - U$) color between the two sequences in Figure 4(a) is much larger than the photometric uncertainties in the colors, this separation of pixels is not a random effect. The sequences are also not the result of differences in residual reddening, as can be seen by comparing the directions of

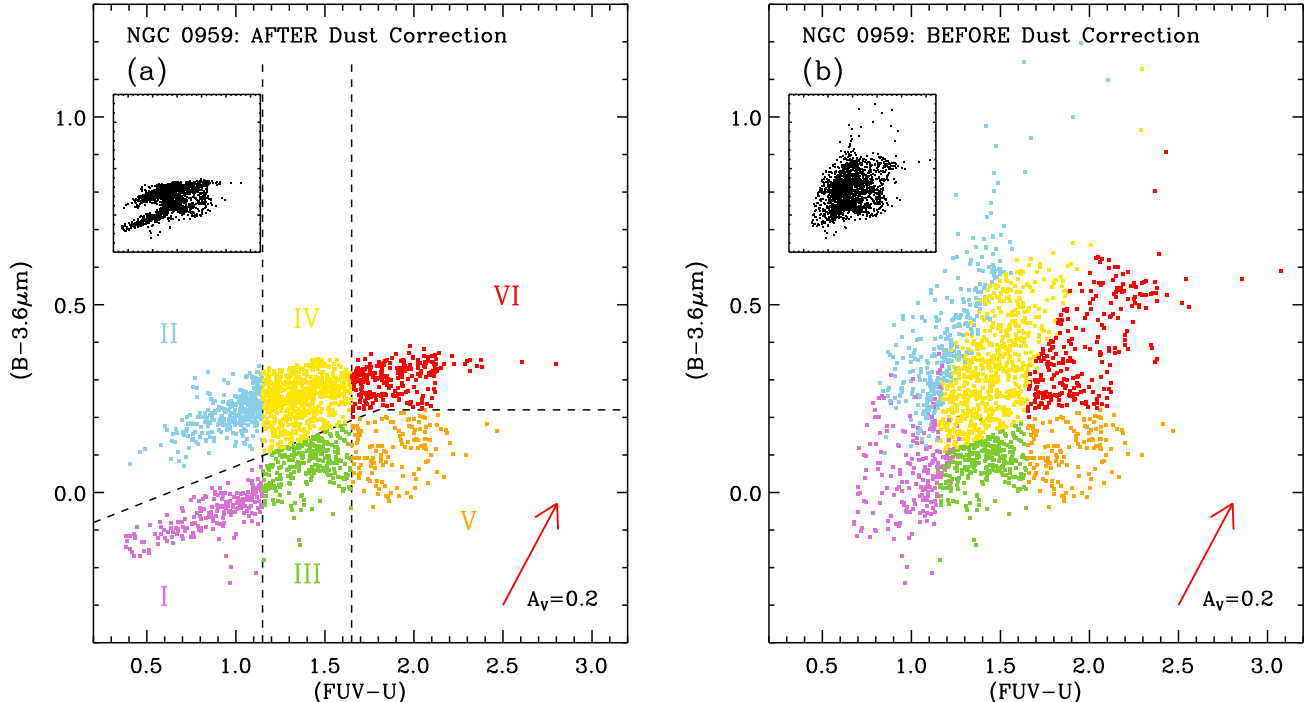


FIG. 4.— Pixel Color-Color Diagrams (pCCDs) of $(B - 3.6 \mu\text{m})$ versus $(FUV - U)$ color for NGC 0959. Panel (a) shows the pCCD *after* our extinction correction (see Paper I) has been applied, while panel (b) shows the pCCD using the *observed* pixel colors. The 25th and 75th percentile uncertainties in color are ~ 0.05 and ~ 0.08 mag in $(B - 3.6 \mu\text{m})$, and ~ 0.01 and ~ 0.02 mag in $(FUV - U)$, respectively. Reddening vectors corresponding to $A_V = 0.2$ mag arcsec⁻² are drawn in the bottom right corners. Pixel groups were selected in panel (a) and retain their group assignment and color-coding in panel (b). Small insets show the pCCDs, plotted over the same color ranges as the main panels, but omitting the color coding that might guide the reader’s eye. While the pCCD before extinction correction shows no prominent well-separated features in color-color space, distinct sequences and pixel groupings appear *after* application of our extinction correction (panel a).

the sequences with that of the reddening vector drawn in Figure 4(a). The red and blue sequences are connected in the $1.15 \lesssim (FUV - U) \lesssim 1.65$ mag color range by pixels with intermediate colors. At colors redder than $(FUV - U) \simeq 1.65$ mag, the pixels again somewhat separate into sequences with redder and bluer $(B - 3.6 \mu\text{m})$ colors.

As can be seen in various SED models (e.g., Bruzual & Charlot 2003; Anders & Fritze-von Alvensleben 2003; Maraston 2005; Kotulla et al. 2009), the $(FUV - U)$ color is very sensitive to age for the youngest stellar populations. Since most of the FUV flux is emitted by young, massive OB-stars, combining a *GALEX* and an optical broad-band filter provides strong age constraints (e.g., Kaviraj et al. 2007). The $(B - 3.6 \mu\text{m})$ color was selected empirically, while examining different combinations of colors. The IRAC $3.6 \mu\text{m}$ bandpass is commonly used as a stellar mass distribution tracer (e.g., Willner et al. 2004), because it is associated more with the distribution of redder and older stars. Since the optical B -band is generally sensitive to younger stars, the $(B - 3.6 \mu\text{m})$ color can be used to distinguish mixtures of stellar populations with and without significant recent high-mass star formation. The combination of $(FUV - U)$ and $(B - 3.6 \mu\text{m})$ colors in Figure 4(a), therefore, provides a powerful diagnostic of the recent star formation history averaged over a pixel.

5.3. Definition of Pixel Groups

Based on the distinct red and blue sequences, as well as transition regions identified in Figure 4(a), we separated pixels into six different groups (color-coded in Figure 4(a)). The group boundaries (selection criteria) are summarized in Table 1. The exact location of the boundaries between some of these pixel groups is somewhat arbitrary, but is motivated by the following considerations.

The Group I pixels (color-coded purple) reside on the blue part of the blue sequence, and have blue colors in both $(B - 3.6 \mu\text{m})$ and $(FUV - U)$. The dominant stellar populations are very young and massive OB-stars, while older stellar populations contribute little to the total flux in these pixels. The $(B - 3.6 \mu\text{m})$ and $(FUV - U)$ colors become redder as these young stellar populations age and the number of remaining OB-stars decreases.

On the other extreme, the Group VI pixels (color-coded red) have red colors in both $(B - 3.6 \mu\text{m})$ and $(FUV - U)$. These pixels are therefore dominated by old, quiescent, “red-and-dead” stellar populations and do not contain a detectable fraction of young, massive stars.

The Group II pixels (color-coded blue) have the same blue $(FUV - U)$ color range as Group I, but redder $(B - 3.6 \mu\text{m})$ colors. The blue $(FUV - U)$ color implies the presence of OB-stars. The redder $(B - 3.6 \mu\text{m})$ color indicates that Group II pixels have a non-negligible contribution to the total light from older (underlying or superposed along the line-of-sight) stellar populations.

Group V pixels (color-coded orange) cover the same,

TABLE 1
GROUP BOUNDARIES IN THE $(B - 3.6 \mu\text{M})$ VERSUS $(FUV - U)$ pCCD OF FIGURE 4(a)

Pixel Group	Color Code	Group Boundary Definition (mag)
Group I	Purple	$(FUV - U) < 1.15$ $(B - 3.6 \mu\text{M}) < 0.188 \cdot (FUV - U) - 0.118$
Group II	Blue	$(FUV - U) < 1.15$ $(B - 3.6 \mu\text{M}) \geq 0.188 \cdot (FUV - U) - 0.118$
Group III	Green	$1.15 \leq (FUV - U) < 1.65$ $(B - 3.6 \mu\text{M}) < 0.188 \cdot (FUV - U) - 0.118$
Group IV	Yellow	$1.15 \leq (FUV - U) < 1.65$ $(B - 3.6 \mu\text{M}) \geq 0.188 \cdot (FUV - U) - 0.118$
Group V	Orange	$(FUV - U) \geq 1.65$ $(B - 3.6 \mu\text{M}) < 0.22$ and $(B - 3.6 \mu\text{M}) < 0.188 \cdot (FUV - U) - 0.118$
Group VI	Red	$(FUV - U) \geq 1.65$ $(B - 3.6 \mu\text{M}) \geq 0.22$ or $(B - 3.6 \mu\text{M}) \geq 0.188 \cdot (FUV - U) - 0.118$

red, $(FUV - U)$ color range as Group VI, indicating that they too lack a detectable fraction of young, massive OB-stars. Yet, their bluer $(B - 3.6 \mu\text{M})$ color suggests that the flux in these pixels is dominated by light from intermediate age stellar populations.

The Group III and Group IV pixels (color-coded green and yellow, respectively) are located between these extreme cases. The light in these pixels is likely dominated by stellar populations in transition between the extreme groups along either blue or red sequences, or between the blue and the red sequence, or represents a mixture of stellar populations (from unresolved adjacent regions or regions superposed along the line-of-sight) with different star formation histories.

5.4. Effect of Pixel-Based Extinction Correction

Figure 4(b) shows the pCCD of $(B - 3.6 \mu\text{M})$ versus $(FUV - U)$ color *before* the application of the extinction correction. For each pixel, the color coding was preserved from that in Figure 4(a). This allows us to track the effect of applying the extinction correction in this color-color space. Interestingly, as shown in the inset of Figure 4(b), once the color coding is removed, obvious features like the blue and red sequences of Figure 4(a) are no longer discernible. The Group I and II pixels, for example, which were clearly separated in Figure 4(a), have blended to form a continuous distribution in Figure 4(b). The main difference between Groups I and II, which both are characterized by the presence of OB-stars, is the fraction of light contributed by older stellar populations. Group III and IV pixels, defined as having $1.15 \leq (FUV - U) < 1.65$ mag *after* extinction correction, are affected differently by the extinction correction (as a comparison of Figures 4(a) and 4(b) shows). Like Group I and II pixels, Group IV pixels are found scattered out to much redder $(B - 3.6 \mu\text{M})$ colors *before* extinction correction. Most of the Group III pixels, on the other hand, can be located in the same color-color space in both panels of Figure 4. The same difference is seen between pixel groups V and VI. This indicates that Group III and V pixels have almost no measurable dust extinction, while Group IV and VI pixels are signif-

icantly obscured by dust. As a side note, the reduction of the scatter going from the observed to the extinction-corrected version of the $(B - 3.6 \mu\text{M})$ versus $(FUV - U)$ pCCD is only possible if the extinction correction applied to each individual pixel was appropriate, at least to first order.

The pixel-averaged dust extinction estimated by our method in NGC 0959 (Figure 1) indeed varies from $A_V = 0.0$ to $A_V \simeq 0.8$ mag arcsec⁻². In Paper I, we also measured the average visual dust extinction across the entire galaxy, $\overline{A_V} = 0.064^{+0.086}_{-0.049}$ mag arcsec⁻², and the azimuthally averaged radial extinction profile, $A_V(R)$, which has a central value of $A_V(R = 0) \simeq 0.25$ mag arcsec⁻², but quickly drops to below $A_V = 0.1$ mag arcsec⁻² beyond a radius of $\sim 0.2 R_{25}$, where R_{25} denotes the major axis radius at the $\mu_B = 25.0$ mag arcsec⁻² isophote (RC3; de Vaucouleurs et al. 1991). These average A_V values are much smaller than the peak pixel-based A_V estimate. Also, while the $\overline{A_V}$ and radial profile do not become zero at any radius, with our method (see Paper I) about $\sim 55\%$ of the analyzed pixels in NGC 0959 have $A_V = 0.0$ mag arcsec⁻² to within the photometric uncertainties.

Before we proceed to the next section, let us consider what might cause the difference in dust extinction between Groups I and III on the blue sequence. Dust and gas are easily removed by starburst heating (e.g., Mihos & Hernquist 1994, 1996) and stellar winds (e.g. Murray et al. 2005), and both mechanisms become stronger as the size of an OB association becomes larger. Therefore, if the dominant stellar populations in Group III pixels are indeed evolved Group I populations wherein OB-stars have died off, we would *expect* them to suffer less extinction, unless some mechanism for rapid reformation and pervasive distribution of dust were at play. Figures 4(a) and 4(b) show that, once dust-free, these populations do *not* become significantly dustier evolving from Group III to Group V, apparently ruling out such rapid reformation. Since we do not observe a similar strong drop in extinction going from Group II to Group IV, we conclude that most of the extinction in those pixels is not physi-

cally associated with the OB-associations themselves, although they could still represent star formation “blisters” on the far side of large molecular cloud complexes.

5.5. *Is NGC 0959 Unique? Application to Other Galaxies*

To determine whether our pixel-based extinction correction can be used as a general method, or whether NGC 0959 is a special case, we applied the same method to NGC 7320 (SA(s)d at $D = 14.0 \pm 1.0$ Mpc, sampling $102 \times 102 \text{ pc}^2 \text{ pixel}^{-1}$) and UGC 10445 (SBc at $D = 20.0 \pm 1.4$ Mpc, $146 \times 146 \text{ pc}^2 \text{ pixel}^{-1}$), which, although more distant, are selected from our larger sample of 45 galaxies with FUV through mid-IR imagery as relatively close analogs. A more detailed analysis of the distribution of extinction and the intrinsic stellar populations of these galaxies will be performed in Tamura et al. (2010; Paper III, in preparation). Here we simply compare their ($B - 3.6 \mu\text{m}$) versus ($FUV - U$) pCCDs *before* and *after* the application of our pixel-based extinction correction, to help validate the current results for NGC 0959.

Figure 5 shows the distribution of the pixels of NGC 7320 and UGC 10445 that meet our S/N criteria in the same color-color space as Figure 4. The main panels show the distributions *after*, the insets show the distributions *before* extinction correction. For each galaxy, both the main panel and inset show the *same* ranges in color. The vertical dotted lines in the insets represent ($FUV - U$) = 0.0 mag. Reddening vectors corresponding to $A_V = 0.2 \text{ mag arcsec}^{-2}$ are drawn in the lower right corners of the main panels. Since the area subtended by a single pixel is larger than was the case for NGC 0959, the blending of light from distinct stellar populations within a single pixel becomes more significant, resulting in less clear separation of blue and red sequences. Yet, different groupings of pixels, analogous to those defined in Figure 4(a) for NGC 0959, are still recognizable in Figure 5 for both galaxies.

5.6. *A Pixel Coordinate Map of Stellar Populations within NGC 0959*

Having shown that application of our pixel-based extinction correction reveals significant groupings of pixels—dominated by different types or mixtures of stellar populations—in the ($B - 3.6 \mu\text{m}$) versus ($FUV - U$) pCCD, our next question becomes whether the spatial distribution of pixels belonging to these pixel groups will reveal meaningful large- and small-scale physical structures within NGC 0959. To address this question, and to study how each pixel group relates to the visual and physical properties of stellar populations, we plot the pixel groups defined in Figure 4(a) onto a two-dimensional pixel coordinate map (Figure 6). Each square in Figure 6 represents a $1''.5 \times 1''.5$ pixel, color-coded according to the pixel group it is a member of. Black dotted contours again trace the *Spitzer*/IRAC $8.0 \mu\text{m}$ PAH emission. We emphasize that each pixel group was defined *without* using any pixel coordinate information. In other words, this is the *first time* that the spatial distribution of pixels belonging to each of the selected pixel groups is revealed.

First and foremost, Figure 6 demonstrates that the dif-

ferent pixel groups are *not* distributed randomly across the face of NGC 0959’s galactic disk, but cluster in well-defined regions. No systematics in the data processing and process of defining the pixel groups would be expected to result in spatial artifacts larger than 3×3 pixels. Since most regions cover much larger contiguous areas, we conclude that also the smallest spatial groupings must be genuine. Since defining the different pixel groups was possible only in the extinction corrected ($B - 3.6 \mu\text{m}$) versus ($FUV - U$) pCCD, a two-dimensional extinction correction is thus crucial to reveal regions with systematically different star-formation histories.

Group I pixels (purple) are found in and around some of the bluest regions in the extinction-corrected color composite of FUV, V , and $3.6 \mu\text{m}$ images (Figure 2(b)), most of which are recognizable as such in the uncorrected, higher resolution, ground-based UVR color composite (Figure 3) as well. Since the stellar populations dominating these pixels are much brighter than those in other regions (Figure 3), these regions must indeed be vigorously star-forming.

Group II pixels (blue) are generally distributed in regions adjacent to the Group I pixels. Each of the regions (b) and (c) of Section 5.1 are found to belong to this pixel group, as well. In particular, much of a more or less linear structure that runs from the NW to SE of the galaxy through its center, with high $8.0 \mu\text{m}$ surface brightness (PAH emission) and signs of higher than average obscuration (Figures 1 and 3), consists of pixels that belong to Group II. These regions have the blue ($FUV - U$) colors characteristic of OB associations, but are redder in ($B - 3.6 \mu\text{m}$), because a larger fraction of the light is contributed by older stellar populations. These observations are consistent with the presence of a stellar bar. Although NGC 0959 has been studied before (e.g., Esipov et al. 1991; Taylor et al. 2005), to our knowledge this bar has not previously been reported. The dust-corrected color composite in Figure 2(b) also suggests that NGC 0959 has a non-negligible bulge or central condensation, that is partially obscured by dust in Figures 2(a) and 3. We suggest, therefore, that its morphological classification be changed from Sdm (RC3; de Vaucouleurs et al. 1991) or Sc/Irr (UGC; Nilson 1973) to SBcd.

An interesting contrast in average stellar population age is revealed by comparing the spatial distributions of Group III (green), Group IV (yellow) and Group V and VI (orange and red) pixels. Whereas Group III pixels are mostly found in the northwestern half of the galaxy, Group V and VI pixels are distributed predominantly toward the eastern and southeastern periphery of the galaxy (although a smaller region of Group V pixels appears along the northern rim). The regions occupied by Group III pixels appear neither particularly blue (actively star-forming) nor red (quiescent) in Figure 2(b), consistent with the idea that intermediate age (a few 100 Myr) stellar populations are the dominant contributors to the flux in these pixels. The extinction map (Figure 1) shows that these pixels suffer no, or at most minimal extinction by dust. The Group V regions correspond to regions that have a smooth appearance without abrupt changes in surface brightness in Figures 2 and 3, and lacking any signatures of dust (Figures 1 and 3). Their

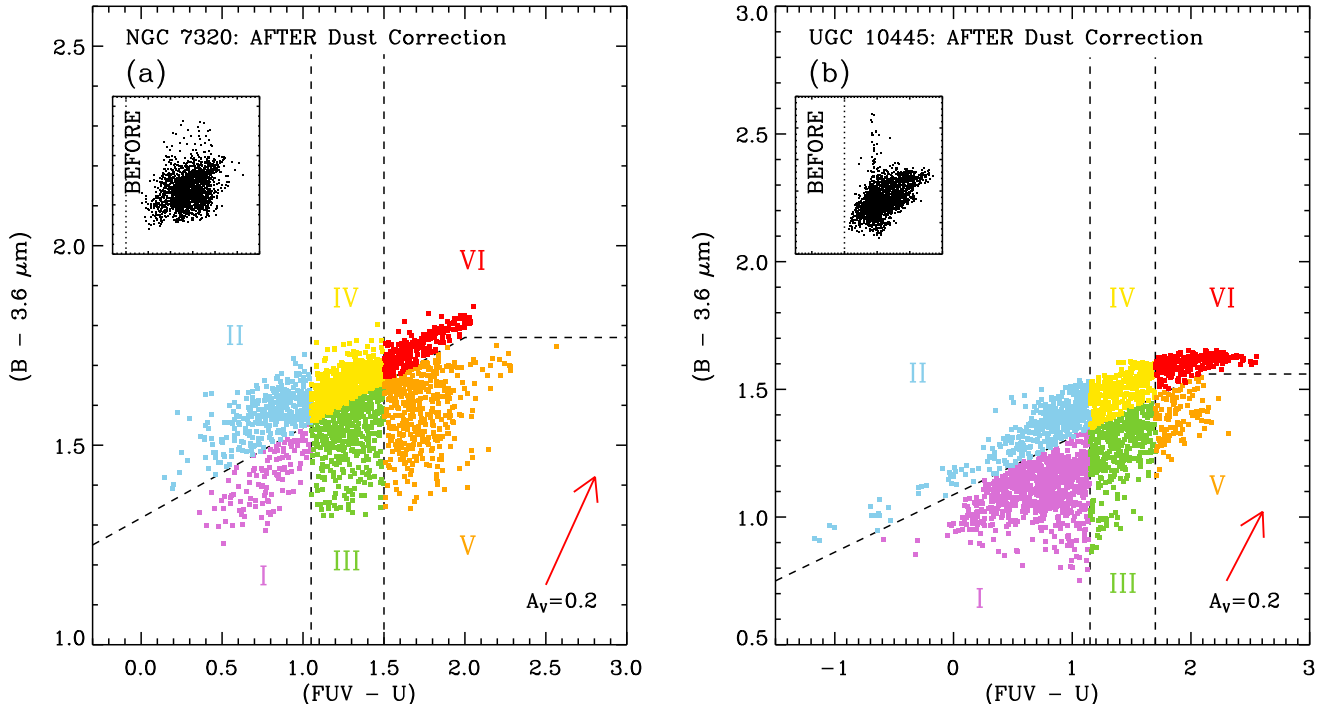


FIG. 5.— Extinction corrected pCCDs for NGC 7320 (SA(s)d, $D = 14.0 \pm 1.0$ Mpc) and UGC 10445 (SBc, $D = 20.0 \pm 1.4$ Mpc), two more distant analogs of NGC 0959 ($D = 9.9 \pm 0.7$ Mpc). Since the area subtended by a single pixel is (much) larger in these galaxies, the effects of light blending are more severe, resulting in smaller and fuzzier separations of red and blue sequences than for NGC 0959. Of course, their star formation histories may also differ. Yet, groupings of pixels that are qualitatively similar to those in NGC 0959 are recognizable in both pCCDs. The insets, plotted over the same color ranges as the main panels for each galaxy, show the distribution of pixels before dust correction. The vertical dotted lines in the inset panels indicate the locations of $(FUV - U) = 0.0$ mag, for comparison with the main panels.

red $(FUV - U)$ colors and neutral $(B - 3.6 \mu\text{m})$ colors indicate that these must be regions with intermediate age ($\sim 1\text{--}2$ Gyr), largely unattenuated stellar populations in the outskirts of the galaxy. The Group VI pixels (red) in the southern half of the galaxy disk suffer some extinction (Figure 1), but the low surface brightness in these regions does not allow one to easily discern dust features in Figures 2 and 3. Even though these regions suffer some extinction, Figure 4(a) demonstrates that these pixels are red mostly because the light is dominated by older (likely older than a few Gyr) stellar populations. The Group IV pixels are distributed throughout the galaxy between the other populations, but perhaps mostly surrounding the Group II pixels. Like Group III, their $(FUV - U)$ colors indicate the presence of relatively young stars and absence of OB-stars, but the redder $(B - 3.6 \mu\text{m})$ colors of Group IV pixels show that a larger fraction of the flux is contributed by older populations. The extinction map (Figure 1) shows that these pixels tend to suffer somewhat less attenuation than Group I and II pixels. The overall impression is that of a large-scale past star-formation episode that started in the south or southeast and propagated toward the northwest, and that is unrelated to the ongoing massive star formation traced by Group I and II pixels, which presently is concentrated more toward the western half of NGC 0959.

The apparent ridge of somewhat higher extinction along the southeastern edge (as defined by our $S/N \geq 3$ criterion) of NGC 0959, so striking in the extinction map (Figure 1), might hint at the presence of either a warp

in the galactic disk or an outer spiral arm delineated by a dust lane. In either case, no significant star-formation must have been associated with that portion of the galactic disk for the past few Gyr.

Concerning the SE-to-NW stellar population gradient of NGC 0959 and its SE extinction ridge, it is worth noting that NGC 0959 is a member of the NGC 1023 galaxy group, which contains 12 other major galaxies (Tully 1980). The center of that group is located $\sim 1.6^\circ$ (~ 240 kpc at $D \simeq 10$ Mpc) south of NGC 0959. The group environment and/or gravitational interaction with NGC 0949—the group member nearest in projection on the sky—may well have played a role in producing the extinction ridge and the stellar population gradient in the disk of NGC 0959. We believe this certainly deserves further study.

6. SUMMARY AND CONCLUSIONS

We have presented the results of a study of NGC 0959 using color composite images, a pCCD, and a pixel coordinate map, and demonstrated the importance and potential of a pixel-based extinction correction. Our study combined ground- and space-based surface photometry, ranging in wavelength from the far-UV (*GALEX*) through mid-IR (*Spitzer*/IRAC). Among the possible combinations of color-magnitude and color-color diagrams examined, we found that the $(B - 3.6 \mu\text{m})$ versus $(FUV - U)$ pCCD proved the most powerful diagnostic of differences in the stellar populations contributing to the flux in a pixel. After applying the pixel-based, two-dimensional extinction correction described in Paper I,

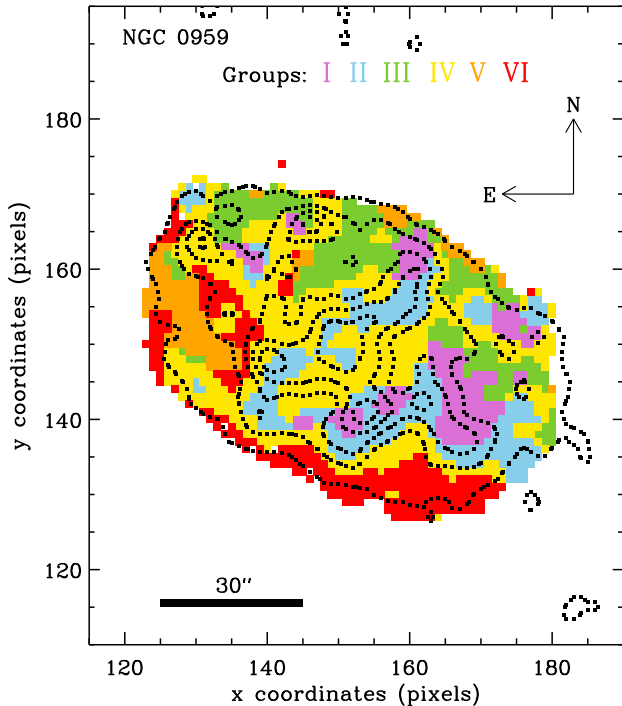


FIG. 6.— Pixel coordinate map of NGC 0959, showing the spatial distribution of pixels belonging to the different pixel groups selected in Figure 4(a), i.e., *after* application of our pixel-based extinction correction. Each square represents a single $1''.5 \times 1''.5$ pixel. The black dotted contours trace the *Spitzer*/IRAC 8.0 μm emission. Group I (purple) and Group II (blue) pixels appear to define some large-scale structure in the galactic disk, highlighted by OB-associations. Especially, Group II pixels reveal a *previously unrecognized* bar-like structure, running from NW to SE across the galaxy center.

we defined six different pixel groups in this diagnostic diagram, ranging from pixels for which both ($FUV - U$) and ($B - 3.6 \mu\text{m}$) colors indicate that their fluxes are dominated by very young, massive stellar populations, to pixels that appear to sample only light from evolved stellar populations. We demonstrated that it was not possible to meaningfully define such pixel groups *before* extinction correction. We then showed that pixels that belong to a given pixel group form well-defined, contiguous regions in a pixel coordinate map, revealing systematic spatial variations in the dominant stellar populations that would not be readily discernible without a two-dimensional correction for extinction. We were able to

report the presence of a previously unrecognized stellar bar, for example.

Our pixel-based two-dimensional method to correct for extinction, based on only $3.6 \mu\text{m}$ and V -band images (adding U improves fidelity), has the advantage that it is applicable to any galaxy that is significantly resolved at rest-frame $\sim 3.6 \mu\text{m}$ and that it is not restricted to a few individual sightlines within a galaxy, nor to the very nearest galaxies. Although seemingly simple and crude, we have demonstrated that application of this method allowed us to uncover relatively detailed spatial information on the nature of stellar populations and on the star formation history within NGC 0959, despite significant spatial variations in the attenuation by intervening dust.

While the spatial resolution in the present study was limited by the *GALEX* NUV PSF of $5''.3$ (FWHM) to linear scales of ~ 250 pc, in the near future, combination of *HST*/WFC3 and *JWST* will provide much higher resolution (FWHM $\simeq 0''.06$ – $0''.11$) at rest-frame UV through mid-IR wavelengths. These instruments will thus allow us to study the distribution of dust extinction and the underlying stellar populations at high fidelity and at much finer spatial resolution within nearby galaxies, as well as at similar scales of a few hundred pc within more distant galaxies. Since galaxies at $z \gtrsim 1$ are important building blocks of the galaxies that we see today at $z \simeq 0$, studying these higher redshift objects with proper two-dimensional extinction estimates will be of significant importance to reveal the nature of galaxy assembly and evolution.

This work is funded by NASA/ADP grant NNX07AH50G and NASA/JWST grant NAG 5-12460. R.A.W. was supported in part by NASA/JWST grant NAG 5-12460. We thank Violet Mager for providing the data observed at the Vatican Advanced Technology Telescope (VATT): the Alice P. Lennon Telescope and the Thomas J. Bannan Astrophysics Facility. We also thank Daniela Calzetti for useful discussions that helped improve our paper. This study has made use of the NASA/IPAC Extragalactic Database (NED), which is operated by the Jet Propulsion Laboratory (JPL), California Institute of Technology, under contract with the National Aeronautics and Space Administration (NASA). This study has also made use of NASA's Astrophysics Data System (ADS). We thank the anonymous referee for constructive comments that helped improve this paper.

REFERENCES

- Anders, P., & Fritze-von Alvensleben, U. 2003, *A&A*, 401, 1063
 Boissier, S., Boselli, A., Buat, V., Donas, J., Milliard, B. 2004, *A&A*, 424, 465
 Boissier, S., et al. 2005, *ApJ*, 619, L83
 Bruzual, G., & Charlot, S. 2003, *MNRAS*, 344, 1000
 Buat, V., & Xu, C. 1996 *A&A*, 306, 61
 Byun, Y.-I. 1992, Ph.D. thesis, Australian National University
 Calzetti, D., Kinney, A. L., & Storchi-Bergmann, T. 1994, *ApJ*, 429, 582
 Calzetti, D., Armus, L., Bohlin, R. C., Kinney, A. L., Koornneef, J., & Storchi-Bergmann, T. 2000, *ApJ*, 533, 682
 Calzetti, D., et al. 2005, *ApJ*, 633, 871
 Calzetti, D., et al. 2007, *ApJ*, 666, 870
 Caplan, J., & Deharveng, L. 1985, *A&AS*, 62, 63
 Clayton, G. C., Gordon, K. D., & Wolfe, M. J. 2000, *ApJS*, 129, 147
 Deo, R., P., Crenshaw, D., M., & Kraemer, S., B. 2006, *AJ*, 132, 321
 de Vaucouleurs, G., de Vaucouleurs, A., Corwin, H. G., Buta, R. J., Paturel, G., & Fouque, P. 1991, *Third Reference Catalogue of Bright Galaxies* (Springer, New York) (RC3)
 Driver, S. P., Popescu, C. C., Tuffs, R. J., Graham, A. W., Liske, J., & Baldry, I. 2008, *ApJ*, 678, 101
 Elmegreen, D. M. 1980, *ApJS*, 43, 37
 Esipov, V. F., Kyazumov, G. A., & Dzhabarov, A. R. 1991, *SvA*, 35, 452
 Fazio, G. G., et al., 2004, *ApJS*, 154, 10
 Gil de Paz, A., et al. 2007, *ApJS*, 173, 185
 Gordon, K. D., & Clayton, G. C. 1998, *ApJ*, 500, 816
 Gordon, K. D., Clayton, G. C., Misselt, K. A., Landolt, A. U., & Wolff, M. J. 2003, *ApJ*, 594, 279

- Kaviraj, S., Rey, S.-C., Rich, R. M., Yoon, S.-J., & Yi, S. K. 2007, *MNRAS*, 381, L74
- Kennicutt, R. C., et al. 2009, *ApJ*, 703, 1672
- Kong, X., Charlot, S., Brinchmann, C., & Fall, S. M. 2004, *MNRAS*, 349, 769
- Kotulla, R., Fritze, U., Weibacher, P., & Anders, P. 2009, *MNRAS*, 396, 462
- Maraston, C. 2005, *MNRAS*, 362, 799
- Martin, D. C., et al. 2005, *ApJ*, 619, L1
- Mathis, J. S., Ruml, W., & Nordsieck, K. H. 1977, *ApJ*, 217, 425
- Mihos, C. J., & Hernquist, L. 1996, *ApJ*, 464, 641
- Mihos, C. J., & Hernquist, L. 1994, *ApJ*, 427, 112
- Misselt, K. A., Clayton, G. C., & Gordon, K. D. 1999, *ApJ*, 515, 128
- Morrissey, P., et al. 2007, *ApJS*, 173, 682
- Mould, J. R., et al. 2000, *ApJ*, 529, 786
- Murray, N., Quataert, E., & Thompson, T. A. 2005, *ApJ*, 618, 569
- Nilson, P. 1973, *Uppsala General Catalogue of galaxies*, Uppsala Obs. Ann., vol. 6 (UGC)
- Oke, J. B. 1974, *ApJS*, 27, 21
- Oke, J. B., & Gunn, J. E., 1983, *ApJ*, 266, 713
- Petersen, L., & Gammelgaard, P. 1997, *A&A*, 323, 697
- Price, S. D., Carey, S. J., & Egan, M. P. 2002, *AdSpR*, 30, 2027
- Regan, M. W., 2000, *ApJ*, 541, 142
- Rieke, G. H., et al. 2004, *ApJS*, 154, 25
- Roussel, H., Gil de Paz, A., Seibert, M., Helou, G., Madore, B. F., & Martin, C. 2005, *ApJ*, 632, 227
- Rudy, R. J. 1984, *ApJ*, 284, 33
- Scoville, N. Z., Polletta, M., Ewald, S., Stolovy, S. R., Thompson, R., & Rieke, M. 2001, *AJ*, 122, 3017
- Skrutskie, M. F., Cutri, R. M., Stiening, R., et al. 2006, *AJ*, 131, 1163
- Tamura, K., Jansen, R. A., Windhorst, R. A. 2009, *AJ*, 138, 1634 (Paper I)
- Taylor, V. A., Jansen, R. A., Windhorst, R. A., Odewahn, S. C., & Hibbard, J. E. 2005, *ApJ*, 630, 784
- Trumpler, R. J. 1930, *PASP*, 42, 214
- Tully, R. B. 1980, *ApJ*, 237, 390
- van Houten, C. J. 1961, *Bull. Astron. Inst. Neth.*, 16, 1
- Valencic, L. A., Clayton, G. C., Gordon, K. D., & Smith, T. L., 2003, *ApJ*, 598, 369
- Viallefond, F., Goss, W. M., & Allen R. J. 1982, *A&A*, 115, 373
- Waller, W. H., Gurwell, M., & Tamura, M. 1992, *AJ*, 104, 63
- Walterbos, R. A. M., & Kennicutt, R. C. 1988, *A&A*, 198, 61
- Whittet, D. C. B., Gerakines, P. A., Hough, J. H., & Shenoy, S. S. 2001, *ApJ*, 547, 872
- Whittet, D. C. B., Shenoy, S. S., Clayton, G. C., & Gordon, K. D. 2004, *ApJ*, 602, 291
- Willner, S. P., et al. 2004, *ApJS*, 154, 222
- Witt, A. N., & Gordon, K. D., 2000, *ApJ*, 528, 799
- Witt, A. N., & Gordon, K. D., 1996, *ApJ*, 463, 681
- Witt, A. N., Thronson, H. A., & Capuano, J. M. 1992, *ApJ*, 393, 611
- Worthey, G. 1994, *ApJS*, 95, 107
- Xu, C., & Helou, G. 1996, *ApJ*, 456, 152